Acta Materialia 189 (2020) 274–283

Contents lists available at ScienceDirect

Acta Materialia

journal homepage: www.elsevier.com/locate/actamat

Full length article

A conformable high temperature nitride coating for Ti alloys

Zhaohe Gao[a], Zhenbo Zhang[a], Xun Zhang[a], Justyna Kulczyk-Malecka[b], Han Liu[a], Peter Kelly[b], Philip J. Withers[a], Ping Xiao[a,*]

[a] Henry Royce Institute, Department of Materials, University of Manchester, Manchester, M13 9PL, UK
[b] Surface Engineering Group, Manchester Metropolitan University, Manchester, M1 5GD, UK

ARTICLE INFO

Article History:
Received 22 October 2019
Revised 21 January 2020
Accepted 19 February 2020
Available online 24 February 2020

Keywords:
Adaptive conformability
Twinning
Interface strengthening
Nitride coating
Oxidation

ABSTRACT

There are many applications including aeroengine design where one would like to operate Ti or its alloys at higher temperatures, but the threat of oxidation or fire remains a longstanding challenge. Here, we have designed a bilayer nitride coating for Ti and its alloys produced by magnetron sputter deposition of a SiAlN coating (1.2 μm thick) along with a Mo interlayer. We have taken advantage of interdiffusion and inter-reaction at the interface during cyclic oxidation at 800 °C to form a layered nitride coating system comprising: a SiAlN top layer, a $TiN_{0.26}$ and Ti_5Si_3 mixed phase interlayer, and a Ti-Mo solid solution. The novel $TiN_{0.26}$ interlayer exhibits adaptive conformability via mechanical twinning, thereby accommodating the thermal mismatch strain between the coating and substrate. This, along with high adhesion, confers excellent thermal cycling life with no cracking, spallation and oxidation of the coating, evident after hundreds of hours of cyclic oxidation (>40 cycles) in air at 800 °C. This work provides a design pathway for a new family of coatings displaying excellent adhesion, adaptive conformability and superior environmental protection for Ti alloys at high temperature.

1. Introduction

Ti and Ti alloys are widely used in the aeroengine gas turbine (e.g. fan blade, compressor, etc.) and automotive industries as well as for medical implants due to their low density, high specific strength and excellent corrosion resistance [1–8]. Increasing the gas turbine inlet temperature can increase engine efficiency and thereby increase fossil fuel efficiency [3]. However, Ti alloys have inadequate oxidation resistance during high temperature exposure, which restricts their application. Degradation is characterized by the formation of a rapidly growing, less protective scale of rutile TiO_2 or TiO_2+Al_2O_3 mixtures and a brittle oxygen-rich sublayer (oxygen absorbed layer with enhanced propensity of cracking) beneath the oxide scale, especially at temperatures above 500 °C [9–13]. In order for Ti alloys to be safely applied at higher temperature, various techniques have been used to improve the oxidation resistance by bulk alloying, surface treatments and coating technologies. Of these, coating methods have been found to be the most effective way to improve the oxidation resistance [9,13–17].

Coatings of several types of material have been applied previously, including aluminides, silicides, glass-ceramics and nitrides [12,18–23]. Among the numerous oxidation resistance materials, aluminide and silicide coatings are widely used to provide high temperature protection due to their propensity for forming protective oxide films at the surface. Nevertheless, the aluminide and silicide coatings can degrade by depletion of aluminium and silicon, which are consumed by oxide scale formation and inward diffusion into the Ti substrate during long time exposure at elevated temperatures [9,13,15]. Due to the chemical incompatibility between these types of coatings and Ti or Ti alloy substrates, a brittle phase can form along the coating/substrate interface and, thus, degrade the mechanical properties of the interface [15]. Glass-ceramic (MgO-SiO_2-TiO_2), nitride (TiAlN) and MAX phase (Cr_2AlC) coatings have also attracted considerable interest because of their good chemical stability and excellent high-temperature oxidation resistance [16,21,24]. However, the inherent low ductility of ceramic coatings, poor adhesion and thermal mismatch between the coating and the substrate, especially during in-service cyclic oxidation [25], are areas of great concern restricting their application. All of the above factors mean that despite the number of candidate coatings for the protection of Ti-alloys at high temperature it is worthwhile exploring the potential of new coating systems with the aim of achieving a combination of good adhesion, good spallation resistance, controllable interdiffusion and good oxidation resistance.

Previous studies have shown that SiAlN exhibits excellent oxidation resistance and good thermal stability at high temperature [26–28], but the challenge is to engineer good interfacial performance. Traditional routes for improving the adhesion between physical vapour deposited coatings and the substrate have included optimizing the surface of the substrate, applying a bias potential during deposition, or inserting an interlayer and developing a multilayer concept, etc. [29–34]. Annealing or thermal treatments, on the other hand, have been reported to degrade

* Corresponding author.
E-mail address: p.xiao@manchester.ac.uk (P. Xiao).

https://doi.org/10.1016/j.actamat.2020.02.051

the adhesion of coatings owing to interdiffusion, which leads to the formation of brittle phases and voids at the interface, thermal expansion mismatches which may initiate surface cracks and phase transformations within the coating and/or substrate that could result in a weak interface [35–40].

There are many reasons to think that Mo might act as a good interlayer between Ti and SiAlN. Its coefficient of thermal expansion is between that of Ti and SiAlN [41,42], Ti-Mo can form an infinite solid solution, and it has a relatively high diffusivity in Ti at high temperature [43,44]. Thus, employing Mo as an interlayer may alleviate the thermal mismatch between the Ti substrate and the nitride coating, while interdiffusion of Mo into Ti may enhance the adhesion of the coating.

In this study, we have deposited SiAlN coatings (1.2 μm thick) with a Mo interlayer (300 nm) on Ti and Ti6Al4V alloy by magnetron sputtering. We have taken advantage of the interdiffusion between Ti and Mo, and inter-reaction between Ti and Si_3N_4 from the SiAlN coating at the interface during thermal exposure, aiming to build a new generation of coating systems for Ti alloys at high temperature exhibiting strong diffusion bonding and superior oxidation resistance. Uniquely these coatings appear to be highly conformable and thus resistant to spalling during thermal cycling.

2. Experiments and methods

The coatings were deposited on one side of commercially pure Ti and Ti alloy (Ti-6wt%Al-4wt%V) coupons (50 × 50 × 3 mm^3), which had been ground, polished (surface roughness, Ra 60 nm) and ultrasonically pre-cleaned in acetone. Deposition took place by reactive sputtering in a Teer Coatings UDP 350 magnetron sputtering system, described in detail elsewhere [45]. Three vertically opposed unbalanced magnetrons (300 × 100 mm^2) were installed through the chamber walls surrounding a centrally mounted rotating unheated substrate holder. The 99.5% pure Si, Al and Mo targets were fitted to the magnetrons. Prior to deposition, the chamber was evacuated to a base pressure of lower than 1×10^{-3} Pa. The substrates were sputter cleaned by Ar+ ions at a bias voltage of −600 V DC for 15 mins prior to the deposition. The Si, Al and Mo targets were each powered by Advanced Energy Pinnacle Plus power supplies operating in pulsed DC mode at a powers of 700, 300 and 500 W, respectively, and a pulse frequency of 100 kHz (duty cycle = 60%) and a bias of −30 V was applied to the substrate throughout coating deposition. First the pure molybdenum layer was deposited in an argon (~2.1×10^{-3} mbar, 0.21 Pa) only atmosphere prior to the deposition of the SiAlN coating. The argon to nitrogen gas ratio (Ar: 20 sccm, N_2:60 sccm) during the reactive sputter deposition of SiAlN was controlled using mass flow controllers (MKS Ltd.) and by monitoring the partial pressures (~3.0×10^{-3} mbar, 0.3 Pa) of the introduced gases. The substrate was rotated at a speed of 5 rpm during deposition of Mo and SiAlN. For tribological and environmental protection applications, thin coatings of a few micrometres thickness have been commonly used, with the coating thickness being controlled by the coating deposition rate. The deposition rate of SiAlN coating is 9 nm/minute. For practical purposes in these experiments, a maximum run time of 130 min was adopted. Therefore, this gave a thickness of 1200 nm for SiAlN and 300 nm for Mo. Whilst thicker coatings may be desired for commercial applications, from the perspective of developing and characterising new coatings, this was deemed to be sufficient [26,46–48]. The SiAlN-coated coupons (50 × 50 × 3 mm) were cut into smaller rectangular (15 × 15 × 3 mm) pieces using a SiC abrasive cutting blade in a precision cut-off machine (Accutom 5, Struers). These were used for scratch tests and oxidation tests after cleaning with soapy water and acetone.

For coatings having a thickness around 1 μm thick or less, the nano-scratch test shows relatively higher reproducibility and lower sensitivity to testing parameters (loading rate, radius etc.) than the standard scratch test. The nano-scratch test was used to evaluate coating adhesion, with 5 scratches made on each sample. Prior to scratch testing the as-deposited samples were isothermal annealed in a static air furnace at 800 °C for 0.5 h and 3 h, respectively. The coated surface was scratched with a spheroconical diamond indenter with a tip radius of 5 μm and a cone angle of 90° The normal load was continuously increased linearly, from 0 to 450 mN, within a distance of 300 μm and the profiling load was 50 μN. Cyclic oxidation tests were conducted to evaluate the oxidation resistance and adhesion of coatings. The tests were performed in a furnace with an accuracy ±1 °C in static air. The as-deposited samples were directly placed inside the furnace when the temperature stabilised at the targeted temperature of 800 °C and the test duration was 5 h. After this, the samples were taken directly from the furnace at 800 °C, cooled for 10 min at ambient temperature, then returned for the next cycle, continuing up to 200 h (40 cycles).

The composition of the as-deposited SiAlN coating was analysed by focused ion beam – X-ray photoelectron spectroscopy (FIB-XPS, Kratos AXIS Supra). The sample was depth profiled using 5 kV Ar+ ions to sequentially sputter remove surface material. A 2 mm x 2 mm etch crater was created with a 110 μm analysis area in the centre of the etch crater. The cross-sections of the oxidized SiAlN coating samples were investigated by scanning electron microscopy (SEM, FEI, Quanta 650, Magellan HR) fitted with an energy dispersive X-ray spectroscopy (EDS) system, coupled with a focused ion beam (FIB, FEI, Quanta 3D, Helios 660), described in detail elsewhere [45,48]. To observe the microstructure of the as-deposited coatings and oxidized samples in greater detail, thin lamellae of the cross-sections of the coatings were prepared by FIB using the lift-out technique and then examined by transmission electron microscopy (TEM, FEI, Tecnai G2; FEI, Tecnai T30) fitted with an energy dispersive X-ray spectroscopy (EDS) system and advanced TEM (FEI, Talos, F200A) fitted with Super-X-EDS system. The phase distribution across the interlayer and diffusion layer was mapped using transmission Kikuchi diffraction (TKD) performed on an FEI Magellan HR scanning electron microscope. The 3D distribution of phases and voids across the interdiffusion zone was studied by FIB/SEM slice-and-view. A dual beam workstation (FEI, Quanta 3D) equipped with a FIB column employing a Ga liquid metal ion source, combined with a high resolution field emission scanning electron microscope was used to perform serial cross-sections through the selected volume (10 × 8 × 5 μm). The milling current was 0.3 nA and the voxel size was 80 nm, which set the distance between individual cross-sections imaged by SEM. The stack of cross-sectional SEM micrographs (2048 × 1768) was reconstructed into 3D volume image using Avizo 9.4 software.

3. Results

3.1. As-deposited SiAlN/Mo coating

The as-deposited SiAlN coating is smooth and about 1.2 μm thick, there is no significant porosity or cracking and the 300 nm molybdenum layer deposited between the SiAlN coating and Ti substrate is fully dense, as shown in Fig. 1a. The selective area diffraction (SAD) pattern of the SiAlN coating shows a diffraction halo, as shown in Fig. 1a inset, which indicates that this coating is amorphous. The top surface of the as-deposited SiAlN coating was milled by Ar+ ions and the XPS quantification is performed after each etch cycle, as shown in supplementary Figure s1. The composition of the SiAlN coating is Si: ~40 at%, Al: ~8 at%, N: ~46 at% with the remainder Ar, possibly arising from the XPS sputtering gas or sputtering gas entrained during coating deposition. Elemental distributions across the SiAlN coating are uniform (in the vertical out-of-plane direction). Based on the binding energy, the SiAlN coating is composed of Si_3N_4 and AlN phases [49,50]. The AlN phases are dispersed in the Si_3N_4 matrix, as shown by HAADF image in Fig. 1b. It is also evident that both AlN and Si_3N_4 are amorphous based on the HRTEM and corresponding FFT pattern in Fig. 1c and inset.

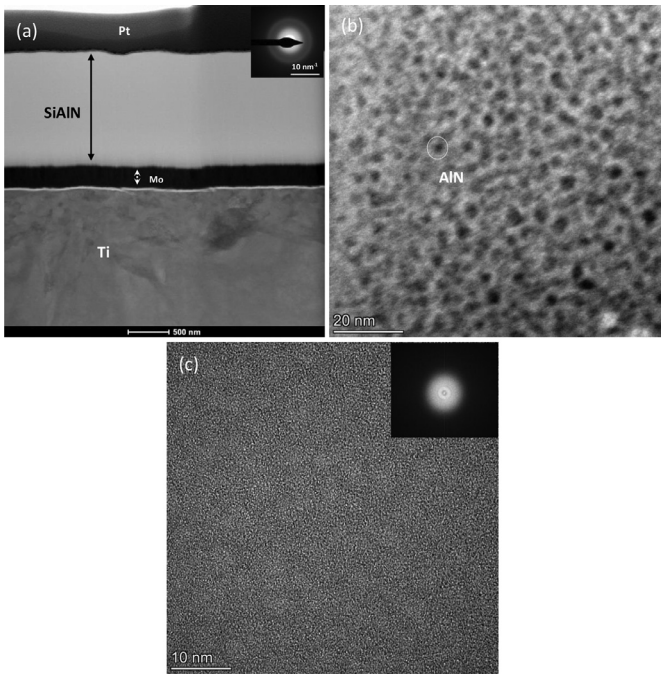

Fig. 1. Microstructure of as-deposited SiAN/Mo coating. (a) Cross-sectional STEM images of as-deposited SiAlN/Mo coating on Ti with diffraction pattern of the SiAlN inset; (b) HAADF image of as-deposited SiAlN coating; (c) HRTEM image of as-deposited SiAlN coating; the inset in (c) shows the FFT pattern.

3.2. Adhesion and oxidation resistance

The as-deposited SiAlN coatings with a Mo interlayer on Ti or Ti6Al4V alloy were exposed to air at 800 °C for 0.5 h, 3 h, 100 h (20 cycles) and 200 h (40 cycles) after which the adhesion and oxidation resistance of the coatings have been evaluated. The adhesion has been evaluated as a function of thermal exposure by scratch testing and the results are summarised in Fig. 2a. The critical load, Lc_2, of the as-deposited SiAlN coating indicated that the first sporadic isolated adhesion failure takes place at about 75 ± 5 mN while the critical loads of the SiAlN samples annealed at 800 °C are about 170±6 mN for 0.5 h annealing time and 230 ± 8 mN for 3 h, respectively. The critical load of the coating annealed at 800 °C for 3 h is around 3 times higher than that of the as-deposited coating. This indicates that the adhesion between the SiAlN coating and Ti substrate has been improved significantly after thermal exposure.

The oxidation protection and resistance to degradation under thermal cycling of the as-deposited coating is demonstrated in Fig. 2 (b-c) and Fig. 3 (a-d). After exposure in air at 800 °C for 100 h (20 cycles), no coating spallation has occurred, nor are there any obvious cracks or porosity, or any signs of oxidation present on the Ti surface covered by the coating (Fig. 2b). The Ti6Al4V alloy coated surface (Fig. 2c and inset, Fig. 3b-d) is also free from spallation, cracks and oxidation after 200 h in air at 800 °C (40 cycles). The only notable change is a slight rumpling of the surface in the former case and pronounced rumpling in the latter case. These contrast markedly with an oxide film formed on bare Ti alloy. For instance, Fig. 3b shows that there is approximately 150 μm thick oxide scale formed on the bare Ti6Al4V alloy after cyclic oxidation at 800 °C for 200 h (40 cycles). It is noteworthy that while there is pronounced rumpling of the SiAlN coated alloy surface after hundreds of hours of cyclic oxidation the coating film remains strongly adhered to the substrate. This suggests that the coating system can adaptively deform in response to the roughening of the substrate. It is noteworthy that this layer is enriched with Mo (confirmed by Fig. 5 below), which remains in the vicinity of the top coat rather than diffusing further into the Ti or Ti alloy substrates even after thermal exposure at 800 °C for 200 h, as shown in Fig. 2b and Fig. 2c. The detailed cross-sectional microstructure of coating and interface after cycling oxidation will be explained below.

These scratch and oxidation tests suggest that the adhesion between the SiAlN coating and Ti substrate can progressively strengthen. It shows a crack-free structure, free from spallation, with negligible interdiffusion, and no weight gain (no observed oxide scale) after hundreds of hours of

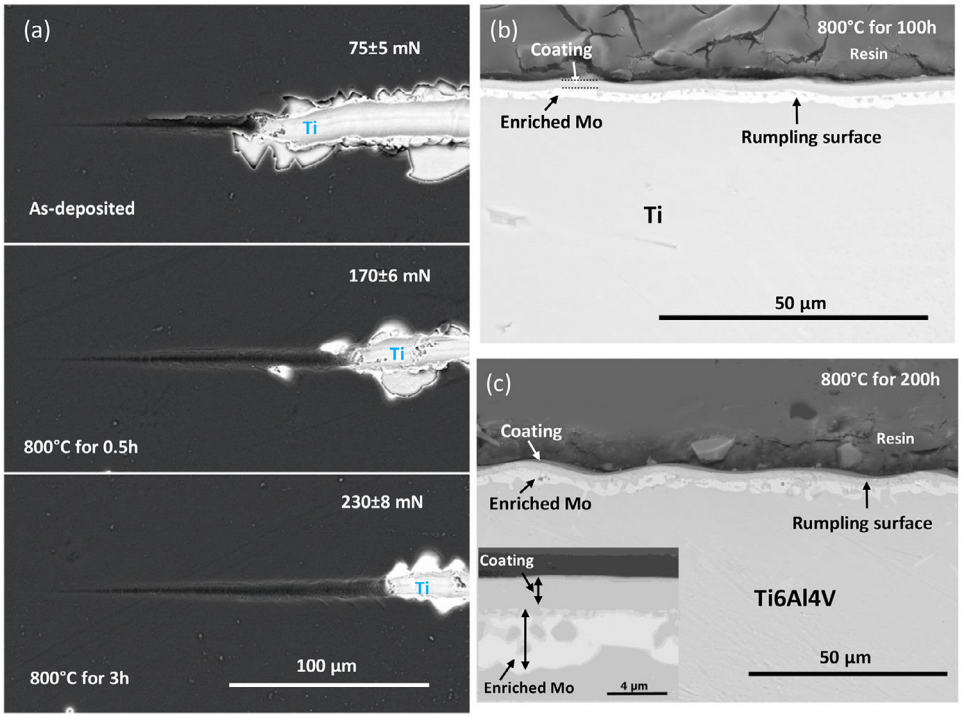

Fig. 2. Interface strengthening and oxidation resistance. (a) Scratch test of as-deposited SiAlN coating with Mo interlayer on Ti substrate and annealed coating at 800 °C in air for 0.5 h and 3 h; (b) The cross-sectional SEM images of SiAlN coating with Mo interlayer on Ti substrate after cyclic oxidation at 800 °C for 100 h in air; (c) The cross-sectional SEM images of SiAlN coating with Mo interlayer on Ti6Al4V substrate after cyclic oxidation at 800 °C for 200 h in air, inset showing the magnified interface.

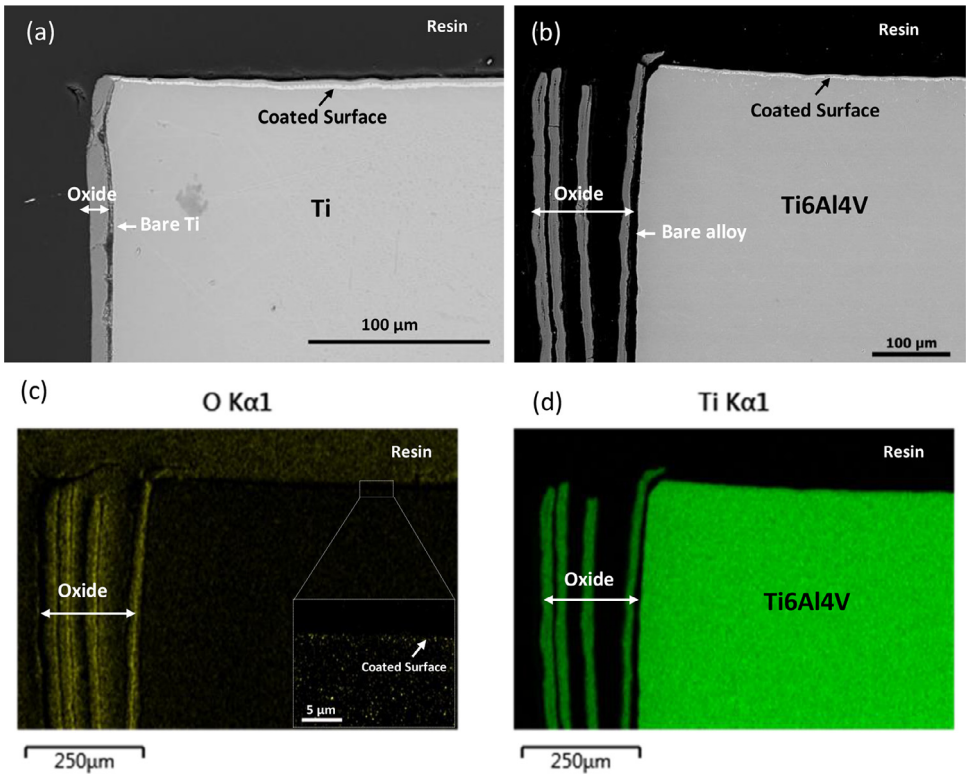

Fig. 3. Oxidation resistance of SiAlN/Mo coating. Cross-sectional SEM image of coated (top side) and bare (left side) surfaces on (a) Ti substrate after cyclic oxidation at 800 °C for 100 h in air; (b) Ti6Al4V substrate after cyclic oxidation at 800 °C for 200 h in air; some of the oxide scale formed on bare alloy exfoliates. (c) and (d) EDS maps for the image in (b), the inset in (c) shows the magnified interface EDS mapping.

cyclic oxidation. This is better than any reported coatings for the protection of Ti alloy. By comparison, SiO_2-Al_2O_3-glass, Cr_2AlC, TiAlN, MgO-SiO_2-TiO_2-glass, TiAl, Al-Si, Cr-Al, TiAlCrY, NiCrCoAl/Al, Al/NiCrAlY, coatings deposited on pure Ti or Ti alloys were tested in static air or by cyclic oxidation from 700 °C to 900 °C [10,12,14,15,18,19,21–23,32,51]. All these coatings demonstrated cracking, spallation or interdiffusion or weight gain problems. For instance; 13 µm interdiffusion thickness and cracking for the glass composite coating after cycling to 800 °C for 100 h [12]; microcracks and spallation for the Cr_2AlC coating at 800 °C for 200 h [10]; a 33 µm thick oxide thickness for $TiAl_3$ coating at 800 °C for 100 h [51].

3.3. Microstructure and constituents after thermal exposure

3.3.1. Coating/substrate interface

To examine the interface strengthening of the SiAlN coating caused by annealing, cross-sections of as-deposited and annealed (at 800 °C for 0.5 h and 3 h in air) coatings have been observed by STEM in Fig. 4. After annealing at 800 °C for 0.5 h, an 300 nm interdiffusion layer forms at the interface between the Mo interlayer and Ti substrate, and a thin diffusion layer (50 nm) between the Mo and SiAlN coating (see Fig. 4b and a). After annealing for 3 h the interdiffusion zone has thickened to 1150 nm and the as-deposited interlayer has transformed into a diffusion zone (see Fig. 4c and e). This arises because the Ti-Mo forms a solid solution allowing the Ti to react with the adjacent Si_3N_4 and AlN phases during annealing (more details on the reaction products below) [43,44,52,53]. Based on the STEM images and EDS elemental maps, the as-deposited interfaces (Mo/Ti, Mo/SiAlN) have transformed to diffusion and reaction zones after annealing at 800 °C.

It can also be observed in Fig. 4c that after annealing there are small numbers of nano-scale pores (40–80 nm in diameter, Kirkendall effect) near to the Ti_5Si_3 intermetallic compounds, distributed in the Mo/Ti diffusion zone underlying the Mo rich layer. In order to track the distribution of intermetallic compounds and pores, a dual-beam focused ion beam-scanning electron microscopy (FIB-SEM) has been used to obtain a 3D reconstruction of the Mo/Ti interface and Mo/SiAlN interface after annealing at 800 °C for 3 h. The Ti_5Si_3 intermetallic compounds marked as red in Fig. 4d, are non-connected and distributed in the diffusion zone underlying the Mo rich layer (Supplementary Video 1 and 3). The nano-scale pores, represented yellow in Fig. 4d, are non-uniformly distributed across the diffusion zone beneath the Mo rich layer (Supplementary Video 1 and 2). Thus, the interdiffusion and inter-reaction of Ti/Mo/SiAlN avoids the accumulation of pores and intermetallic compounds at the coating/substrate interface.

3.3.2. Layered nitride coating

To examine the superior environmental protection and the adaptive deformation of the coating layers, cross sections of the SiAlN coatings after cyclic oxidation were milled by FIB and imaged by SEM, which could provide accurate microstructure details without damaging the coating surface. The cross section of a SiAlN coating/ Mo interlayer on Ti after oxidation at 800 °C for 100 h is shown in Fig. 5a. It is evident that due to interdiffusion and inter-reaction, the original coating/substrate interface has transformed to a complex layered structure. To view this in finer detail, thin lamellas of the cross-section of the coating were prepared by FIB using the lift-out technique and then analysed by STEM, EDS and TKD, as shown in Fig. 5b, c and d. During oxidation at 800 °C for 100 h, the Ti reacts with Si_3N_4 and AlN (SiAlN consisting of Si_3N_4 and a minor amount of AlN), and so there is no excess Si and Al nor depletion of N. This gives rise to a layered structure comprising (from top to bottom): a SiAlN layer, a nanoscale $TiN_{0.26}$ and Ti_5Si_3 mixed layer, a $TiN_{0.26}$ layer, a discontinuous Ti_5Si_3 layer (confirmed by TKD and below HRTEM), and a Ti-Mo solid solution layer. The reaction products between Ti and Si_3N_4 are $TiN_{0.26}$ (hcp, lattice parameter $c/a = 1.6207$) and Ti_5Si_3 as shown below in equations I and 2, confirmed by TKD and HRTEM (Fig. 5 and Fig. 8). It has been reported that the solid solution for TiN_X extends to a maximum value of $x = 0.2$ such that

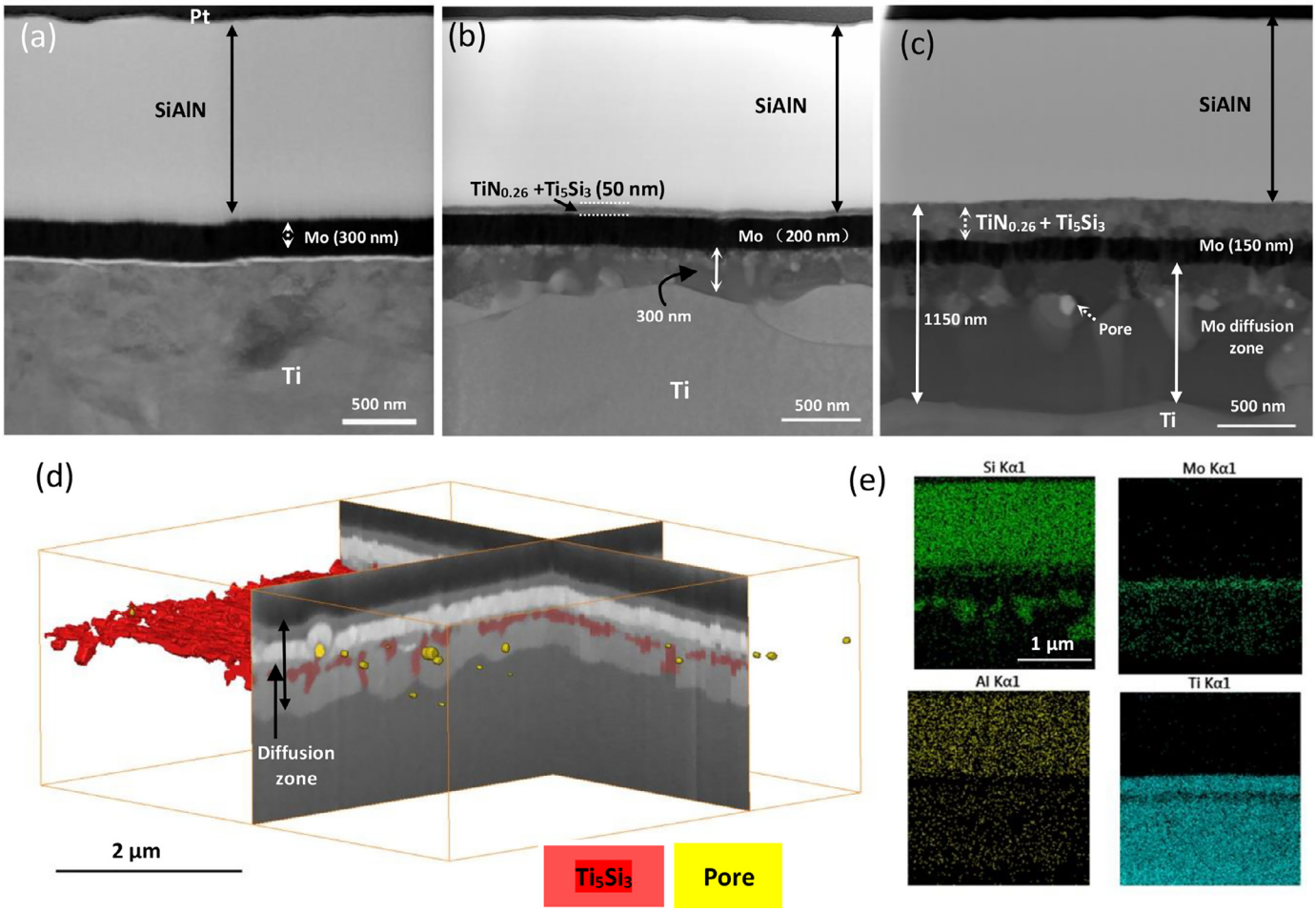

Fig. 4. Microstructure and element distribution of scratch tested samples. Cross-sectional STEM images of SiAlN/Mo coating on Ti, (a) as-deposited SiAlN coating; (b) after annealing at 800 °C in air for 0.5 h; (c) after annealing at 800 °C in air for 3 h; (d) A 3D reconstruction of the SiAlN/Mo and Mo/ Ti interface after annealing at 800 °C in air for 3 h (Ti_5Si_3 is shown in red, pores in yellow); (e) EDS mappings for the image in (c). (For interpretation of the references to colour in this figure legend, the reader is referred to the web version of this article.)

$TiN_{0.26}$ nitride belongs to an hcp structure. The c/a value of $TiN_{0.26}$ is higher than that of $TiN_{0.2}$ as the incorporation of nitrogen atoms caused a continuous increase in c/a value [54]. Similar phases at the interface between Ti and Si_3N_4 have been reported previously [52,55–57]. It is noteworthy that the $TiN_{0.26}$ layer between the substrate and SiAlN coating may serve as a diffusion barrier to mitigate further inter-reaction between Ti and SiAlN, which maintains the chemical and structural compatibility of SiAlN. It can be confirmed that the remnant SiAlN coating (about 450 nm thick) is still amorphous after oxidation at 800 °C for 100 h as shown in the inset image in Fig. 6a and HRTEM image in Fig. 6b. During the Ti/Si_3N_4 reaction, a discontinuous Ti_5Si_3 region (confirmed by Fig. 5c Si element mapping) is formed and mainly distributed between the $TiN_{0.26}$ layer and Ti-Mo solid solution layer. Moreover, Si partly diffuses in the Ti-Mo solid solution and reacts with Ti, which could explain the distribution of Ti_5Si_3 compounds in the Ti-Mo solid solution [57–59]. The reaction between Ti and a trace amount of AlN forms the $TiN_{0.26}$ and Ti(Al) solid solution (Fig. 4e Al and Ti elements distribution), see Eq. (3) [60]. It also can be confirmed that the Al is lean in the $TiN_{0.26}$ or Ti_5Si_3 layer and it distributes into the underlying Ti as a solid solution after oxidation at 800 °C for 100 h, as shown by EDS in Fig. 5c and also verified by Super-X-EDS in supplementary Figure s2. Based on EDS mapping of elemental N in Fig. 5c, it looks like N diffuses into the underlying Ti substrate (Ti-Mo layer) after oxidation at 800 °C for 100 h. But compared with the relative counts of N in the SiAlN and $TiN_{0.26}$ coating areas, the counts of N are lean in the underlying Ti substrate. This has also been corroborated by Super-X-EDS mapping on N in supplementary Figure s2.

$$Ti + 0.065Si_3N_4 = 0.195Si + TiN_{0.26} \quad \Delta G(1073.15K) = -1.825 \times 10^4 J/mol \tag{1}$$

$$5Ti + 3Si = Ti_5Si_3 \quad \Delta G(1073.15K) = -8.16 \times 10^5 J/mol \tag{2}$$

$$Ti + AlN \rightarrow Ti_{1-x}Al_x + TiN_{0.26}\Delta G(1073.15K,\ X = 0.15,\ 0.15\ \text{max solid solution}) = -2.93 \times 10^3 J/mol \tag{3}$$

The inter-reaction product, $TiN_{0.26}$, is mainly distributed beneath the SiAlN coating while the discontinuous Ti_5Si_3 is mainly distributed between the $TiN_{0.26}$ layer and Ti-Mo solid solution layer. Thus, the as-deposited SiAlN/Mo coating has developed into a complex layered nitride coating through a combination of interdiffusion and inter-reaction after extended high temperature exposure, as shown in Fig. 7.

3.3.3. Mechanical twinning

To understand why this novel coating structure is able to adapt to the changes that take place during many thermal cycles without debonding, the microstructure of the coating after cyclic oxidation at 800 °C for 100 h has been characterised in finer detail, as shown in Fig. 8. A high density of planar defects are observed in the $TiN_{0.26}$ layer (Fig. 8a) after cyclic oxidation. We have confirmed that the layer is

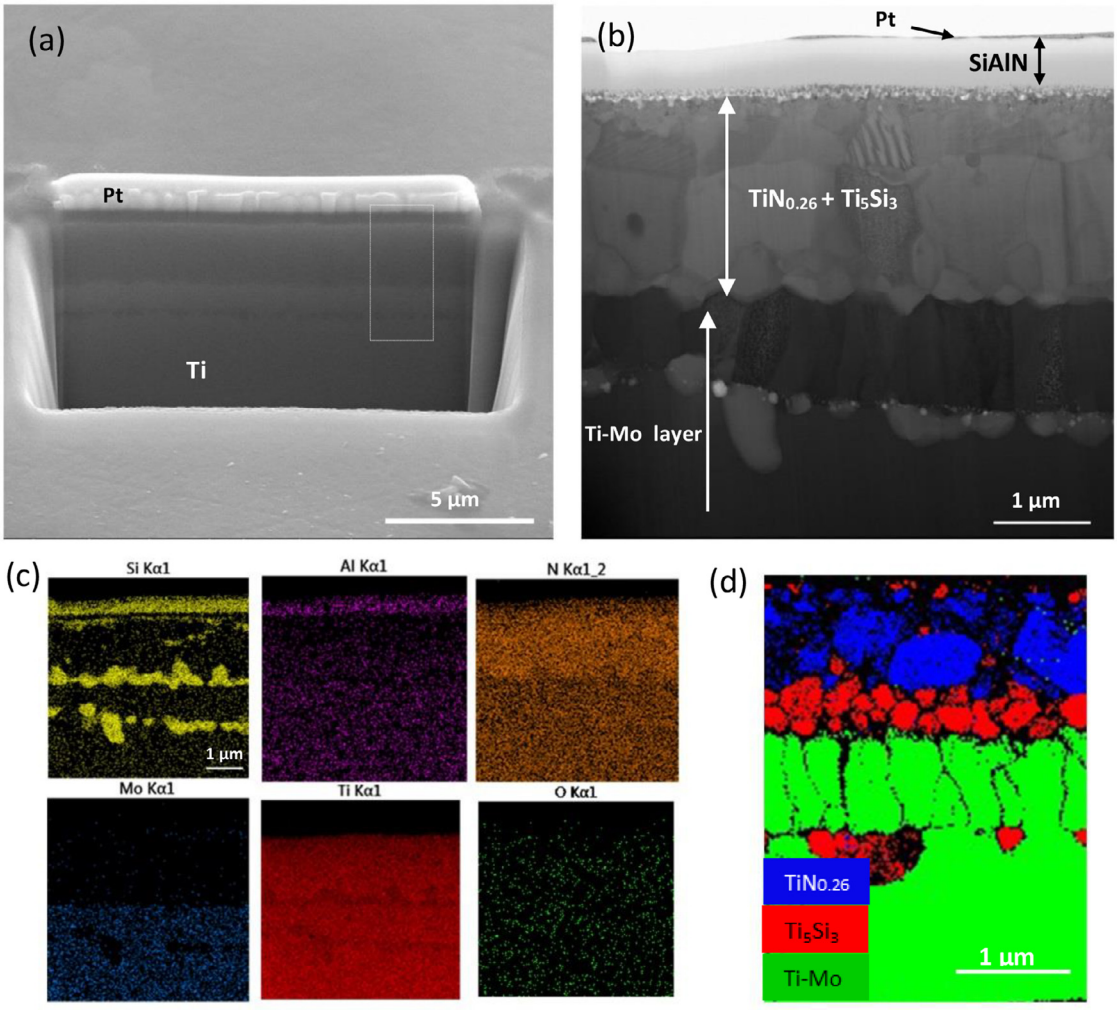

Fig. 5. Microstructure and element distribution for cyclic oxidized samples. (a) Cross-sectional SEM image (tilting 52°) of SiAlN coating with Mo interlayer on Ti after oxidation in air at 800 °C for 100 h; (b) Cross-sectional STEM image of SiAlN/Mo coating on Ti after oxidation in air at 800 °C for 100 h; (c) EDS elemental maps of the region (b); (d) TKD phase map of cross-sectional SiAlN/Mo coating on Ti after oxidation in air at 800 °C for 100 h (Ti-Mo solid solution layer is shown in green colour, Ti_5Si_3 is shown in red colour, $TiN_{0.26}$ is shown in blue colour; white box area in (a) for TKD analysis). (For interpretation of the references to colour in this figure legend, the reader is referred to the web version of this article.)

$TiN_{0.26}$ rather than TiAl by EDS (Al is lean in this layer) and HRTEM analysis (HCP structure instead of cubic TiAl). Analysis based on the HRTEM images in Fig. 8b-g shows that multiple deformation twins formed in the $TiN_{0.26}$, with one set on the scale of several tens of nanometers (Fig. 8b), and the other just a few atomic layers (Fig. 8d-g). The twins can be indexed as {10−11}<10−1−2> twins, based on the FFT pattern in Fig. 8e. In addition, plenty of stacking faults along {10−11} planes accompany the second sets of twins, as shown in Fig. 8g. The formation of deformation twinning and stacking faults in $TiN_{0.26}$ suggests that this layer is able to adaptively deform during the thermal cycles. This enables the $TiN_{0.26}$ layer to accommodate the deformation and reduce the stress between the coating layers, and thereby significantly reduce the susceptibility of the coating to debonding.

4. Discussion

4.1. Interface strengthening

We have seen that the adhesion of the coating after annealing at 800 °C in air for 0.5 h and 3 h is better than that of the as-deposited coating. The primary mechanism of adhesion can be simply divided into two groups: 1) mechanical interlocking, and 2) chemical bonding [30,61,62]. Very often, one of the mechanisms plays a dominant role. During annealing or oxidation at 800 °C, atomic interdiffusion between the Ti substrate and the Mo interlayer occurs, resulting in the formation of a solid solution, as shown in Fig. 4b, c and e. Due to the relatively high diffusivity of Mo in Ti (2.38×10^{-14} cm^2/sec, at 800 °C) and the complete solubility between Mo and Ti [43,44], the Ti-Mo interdiffusion zone can rapidly form giving an interdiffused layer as thick as 300 nm after treating at 800 °C for only 0.5 h. The interface reaction products $TiN_{0.26}$ and Ti_5Si_3 intrude around the bottom of the remnant SiAlN coating, as shown in Fig. 4b, c and Fig. 6. Thus, the as-deposited Mo/Ti and Mo/SiAlN interfaces represent chemically bonded interfaces. On other hand, interdiffusion of elements during annealing or thermal treatments can also degrade the adhesion of coatings. This is because interdiffusion can potentially result in the formation of brittle phases and voids at interface, along with thermal expansion mismatches between the coating and substrate, which promote surface crack initiation and interfacial decohesion [35–40]. However, in our designed layered nitride coating system, the pores do not show agglomeration nor does a continuous brittle intermetallic form at the interface. It is evident (Fig. 4d) that the small numbers of nano-scale pores induced by the Kirkendal effect are mainly non-uniformly distributed inside the Ti-Mo solid solution, and no continuous Ti_5Si_3 phases is formed at the interface. Therefore, the chemical bonding via interdiffusion and interreaction confers our coating enhanced adhesion after short annealing times or hundreds of hour's cyclic oxidation.

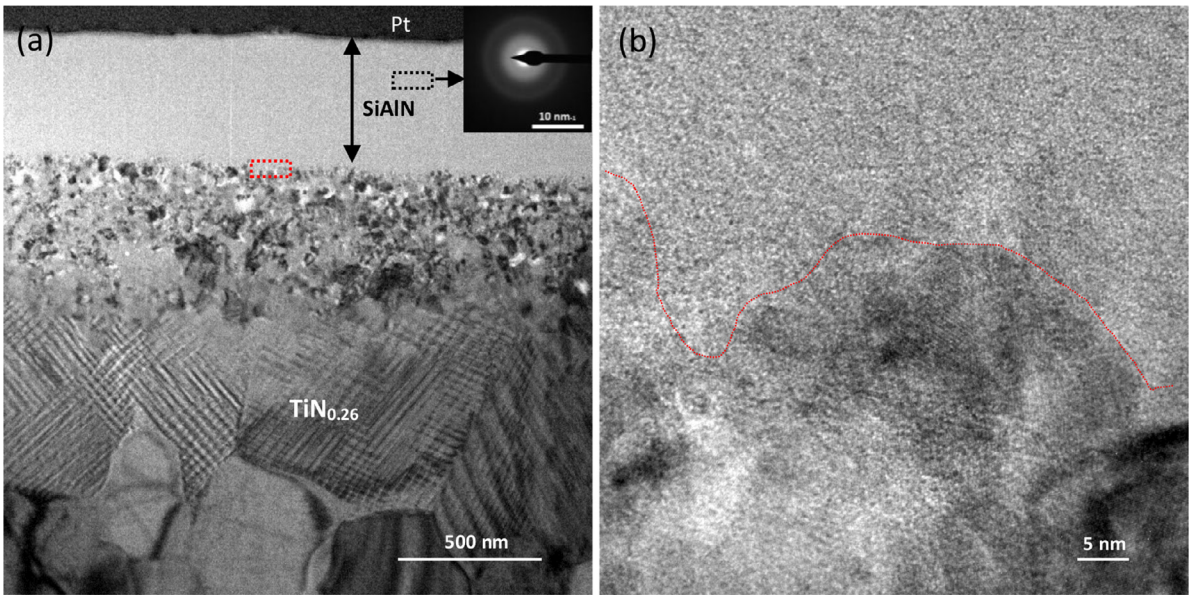

Fig. 6. Microstructure of SiAlN coating after 100 h oxidation. (a) Cross-sectional TEM image of SiAlN coating with Mo interlayer on Ti after oxidation at 800 °C for 100 h, The inset in (a) shows the diffraction pattern of SiAlN coating; (b) HRTEM image of the red box in (a) (top of the dashed red line indicates the remnant SiAlN coating). (For interpretation of the references to colour in this figure legend, the reader is referred to the web version of this article.)

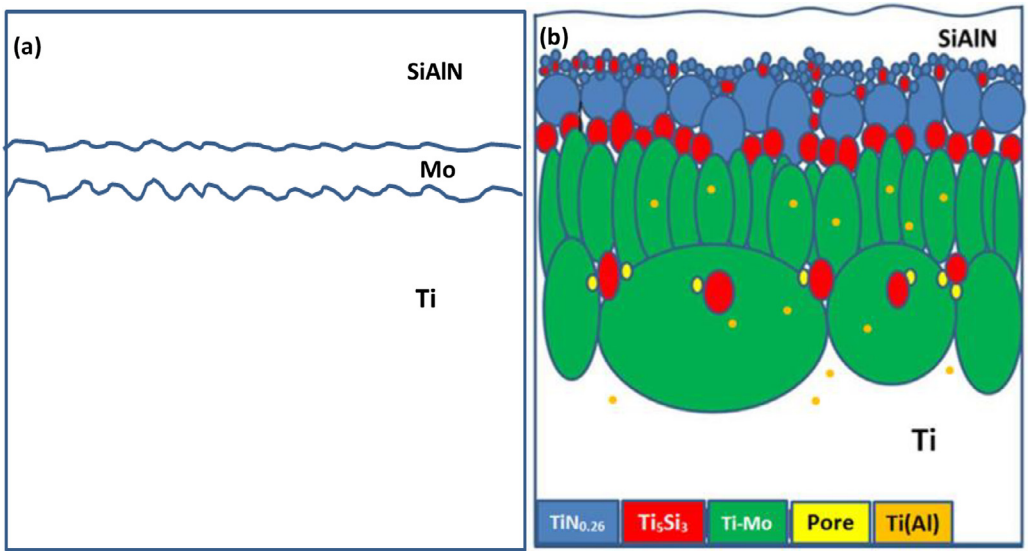

Fig. 7. Schematic diagrams of as-deposited and layered nitride coating system. (a) Schematic diagram of as-deposited SiAlN/Mo coating; (b) Schematic diagram of layered coating system after interdiffusion and interaction (Ti_5Si_3 is shown in red, pores in yellow, Ti-Mo solution in green, Ti(Al) solution in orange and $TiN_{0.26}$ in blue). (For interpretation of the references to colour in this figure legend, the reader is referred to the web version of this article.)

4.2. Adaptive conformability via mechanical twinning

During cyclic thermal oxidation, compressive stresses develop from thermal mismatch between the SiAlN (Si_3N_4 = 3.2 μm/(m·K)) coating and the Ti substrate (8.6 μm/(m·K)) during cooling [41,57]. In addition, after extended periods at high temperature, the growth of the solid reaction layers ($TiN_{0.26}$, Ti_5Si_3) between the SiAlN layer and the Ti substrate results in a volume expansion. Therefore it is essential to alleviate this stress/strain to maintain the coating system integrity and avoid cracking and spallation. In our layered nitride coating system, the deformable $TiN_{0.26}$ layer helps to overcome this problem via mechanical twinning and stacking faults (Fig. 8). Such adaptive deformability during thermal exposure is able to mediate and release the stress/strain, and thereby effectively reduces the debonding susceptibility and prolongs the cyclic lifetime during oxidation tests at high temperatures.

4.3. Oxidation protection mechanism

The conformal complex layered nitride coating appears to provide excellent protection for the Ti and Ti alloy substrate at 800 °C with no oxide observed by SEM and STEM, no cracks and no spallation, confirmed by Figs. 2, 3 and 5. It is well known that the protection mechanism of a metallic substrate by thin coatings against oxidation at high temperature can be affected by intrinsic oxidation resistance of the coating, the chemical compatibility of the coating (e.g. no interdiffusion with underneath substrate) and the coating-substrate integrity (no cracks and no spallation) [26,63]. It has been reported that TmN/Si_3N_4 (Tm = Zr, Al, Ti, Cr, Ta) nanocomposite nitride coatings consisting of a stable amorphous Si_3N_4 phase and the TmN phase exhibit good high temperature oxidation resistance [26–28,64–66] even up to 1300 °C (heating rate at 10 °C/min and immediately cooling to RT upon reaching 1300 °C) when (Tm = Al, Ta, Ti) [26,67]. For the SiAlN

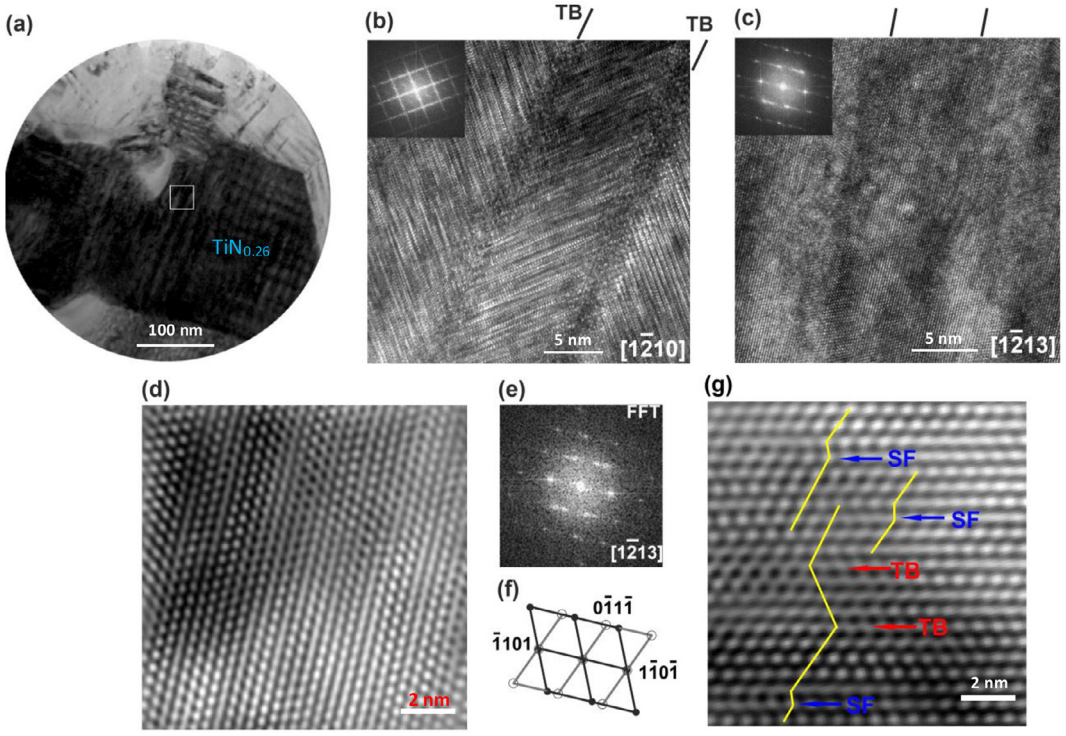

Fig. 8. Microstructure of $TiN_{0.26}$ phase in the layered coating system after cyclic oxidation at 800 °C for 100 h. (a) An overview TEM image of several $TiN_{0.26}$ grains; (b) A HRTEM image with the incident electron beam along [1-210] zone axis from the framed region in (a) with an inset showing the corresponding Fast Fourier Transform (FFT), and twin boundary (TB) is marked; (c) A HRTEM image with the incident beam along [1-213] zone axis; (d) A magnified image from (c) showing the $TiN_{0.26}$ lattice along [1-213] zone axis; (e) The FFT pattern of the image (d) and its corresponding indices (f) showing the existence of twin; (g) An enlarged HRTEM image from (d) with stacking fault (SF) and TB indicated by blue and red arrows, respectively. (For interpretation of the references to colour in this figure legend, the reader is referred to the web version of this article.)

coating, the desired morphology of AlN/Si_3N_4 should be AlN nanoparticles dispersed in an amorphous Si_3N_4 matrix. It has been reported that at Si concentrations larger than 12 at%, the SiAlN coating has the desired nanocomposite structure [67]. In our case the SiAlN (AlN/Si_3N_4 with a Si content at 40 at%) top layer belongs to the family of TmN/Si_3N_4 (Tm = Zr, Al, Ti, Cr,Ta) nanocomposite nitrides. During hundreds of hours of high temperature exposure, one would normally expect interdiffusion between SiAlN and the substrate, which could change the chemical composition and degrade the structure of SiAlN and degrade the oxidation resistance of the coating. Indeed, Musil [26] has reported that the diffusion of elements from the underlying substrate to the coating can stimulate the crystallization of amorphous nitride coatings, and thereby decrease the oxidation resistance during thermal exposure. To maintain the chemical compatibility of coating, the interdiffusion should be avoided or mitigated. In our case this is achieved by inserting an interlayer of Mo, since Mo is known to be able to reduce the activity of Ti and also slow down the interfacial reaction [68,69]. Even if the reaction between Ti and SiAlN occurs, the reaction products, $TiN_{0.26}$, are mainly distributed between the substrate and SiAlN coating and are capable of serving as a diffusion barrier to mitigate further interreaction between Ti and SiAlN, which maintains the chemical and structural compatibility of SiAlN. It is confirmed that no diffusion from the underlying Ti into the SiAlN coating happens and the remnant SiAlN coating (about 450 nm thick) is still amorphous after oxidation at 800 °C for 100 h, as shown in Fig. 5c and Fig. 6, respectively. This explains why our coating displays good thermal stability with no oxide scale formed on the coating even after hundreds of hours at 800 °C in air (as confirmed by Fig. 2b, c, Fig. 3 and Fig. 5). The integrity of the coating-substrate system also benefits from mechanical twinning in the $TiN_{0.26}$ interlayer which mediates and releases the stress of coatings, and thereby greatly reduces the debonding susceptibility. Thus, the layered nitride coating system is effective because it develops an enhanced bonding interlayer by interdiffusion, a transition layer with adaptive deformability and controllable interdiffusion, while the SiAlN layer provides oxidation resistance at the free surface. Overall, this appears to deliver excellent protection for Ti and its alloys for up to 200 h at 800 °C.

5. Conclusion

In conclusion, we have designed a bilayer nitride coating for Ti and its alloys produced by magnetron sputtering a SiAlN coating with a Mo interlayer. We have taken advantage of interdiffusion and inter-reaction at the interface during cyclic oxidation at 800 °C to form a complex layered nitride coating system comprising: a SiAlN top layer, a $TiN_{0.26}$ and Ti_5Si_3 mixed phase interlayer, and a Ti-Mo solid solution. Importantly, the layered nitride coating system shows enhanced adhesion after thermal exposure due to the interdiffusion and it can adaptively conform such that upon extensive thermal cycling (up to 200 h, 40 cycles in air at 800 °C) no visible cracking or spallation occurs nor is a visible oxide scale formed. The novel $TiN_{0.26}$ interlayer exhibits adaptive conformability via mechanical twinning, thereby accommodating the thermal mismatch strain between the coating and substrate. More broadly, the SiAlN coating with Mo interlayer could also be exploited for other candidate Ti-alloys and even gamma TiAl intermetallic alloys. Moreover, due to the scalability and relative low-cost of the magnetron sputtering technology, this coating system has potential for large-scale industrial production. Candidate applications include coatings in the hot section components in gas turbines (e.g. mitigating titanium fire), defence and automobile industries. The innovative interface strengthening design via interdiffusion and inter-reaction also can be potentially applied in the coatings in the medical implants fields.

Declaration of Competing Interest

The authors declare that they have no known competing financial interests or personal relationships that could have appeared to influence the work reported in this paper.

Acknowledgments

We are indebted to Prof. Jian Cao, Prof. Yi Zeng, Dr. Ying Chen, Dr. Chun Li and Dr. Tianzhu Sun for the valuable discussion of this work. We are indebted to Dr. Xinxin Zhang, Dr. Patrick Hill for the valuable assistance on the phase identification of this work. PJW is grateful to the European Research Council grant No. 695638 CORREL-CT as well as funding through the Henry Royce Institute for Advanced Materials funded by EP/R00661X.

Supplementary materials

Supplementary material associated with this article can be found in the online version at doi:10.1016/j.actamat.2020.02.051.

References

[1] M. Bönisch, A. Panigrahi, M. Stoica, M. Calin, E. Ahrens, M. Zehetbauer, W. Skrotzki, J. Eckert, Giant thermal expansion and α-precipitation pathways in Ti-alloys, Nat. Commun. 8 (1) (2017) 1429.
[2] G. Chen, Y. Peng, G. Zheng, Z. Qi, M. Wang, H. Yu, C. Dong, C.T. Liu, Polysynthetic twinned TiAl single crystals for high-temperature applications, Nat. Mater 15 (2016) 876.
[3] T.M. Pollock, Alloy design for aircraft engines, Nat. Mater 15 (2016) 809.
[4] Z. Sun, S. Guo, H. Yang, Nucleation and growth mechanism of α-lamellae of Ti alloy TA15 cooling from an $\alpha+\beta$ phase field, Acta Mater 61 (6) (2013) 2057–2064.
[5] S. Challipalli, H.F. Francis, Mechanical alloying of titanium-base alloys, Adv. Mater 5 (1993) 96–106.
[6] Y. Shi, L. Wang, Y. Niu, N. Yu, P. Xing, L. Dong, C. Wang, Fungal component coating enhances titanium implant-bone integration, Adv. Funct. Mater. 28 (46) (2018).
[7] M. Uchida, A. Oyane, H.M. Kim, T. Kokubo, A. Ito, Biomimetic coating of laminin–apatite composite on titanium metal and its excellent cell-adhesive properties, Adv. Mater 16 (13) (2004) 1071–1074.
[8] R.S. Bedi, L.P. Zanello, Y. Yan, Osteoconductive and osteoinductive properties of zeolite MFI coatings on titanium alloys, Adv. Funct. Mater 19 (24) (2009) 3856–3861.
[9] S.Q. Tang, S.J. Qu, A.H. Feng, C. Feng, J. Shen, D.L. Chen, Core-multishell globular oxidation in a new TiAlNbCr alloy at high temperatures, Sci. Rep. 7 (1) (2017) 3483.
[10] Q.M. Wang, A. Flores Renteria, O. Schroeter, R. Mykhaylonka, C. Leyens, W. Garkas, M. to Baben, Fabrication and oxidation behavior of Cr_2AlC coating on Ti6242 alloy, Surf. Coat. Technol. 204 (15) (2010) 2343–2352.
[11] H.L. Du, P.K. Datta, D.B. Lewis, J.S. Burnell-Gray, Air oxidation behaviour of Ti 6Al 4V alloy between 650 and 850°C, Corros. Sci. 36 (4) (1994) 631–642.
[12] W. Li, S. Zhu, C. Wang, M. Chen, M. Shen, F. Wang, SiO_2–Al_2O_3–glass composite coating on Ti–6Al–4V alloy: Oxidation and interfacial reaction behavior, Corros. Sci. 74 (2013) 367–378.
[13] I. Gurrappa, A.K. Gogia, Development of oxidation resistant coatings for titanium alloys, Mater. Sci. Technol. 17 (5) (2001) 581–587.
[14] J. Dai, J. Zhu, C. Chen, F. Weng, High temperature oxidation behavior and research status of modifications on improving high temperature oxidation resistance of titanium alloys and titanium aluminides: A review, J. Alloys Compd 685 (2016) 784–798.
[15] X. Gong, R. Chen, Q. Wang, Y. Wang, N. Zhang, Z. Zhang, H. Fu, Cyclic oxidation behavior and oxide scale adhesion of Al/NiCrAlY coating on pure titanium alloy, J. Alloys Compd 729 (2017) 679–687.
[16] M. Wen, C. Wen, P. Hodgson, Y. Li, Thermal oxidation behaviour of bulk titanium with nanocrystalline surface layer, Corros. Sci. 59 (2012) 352–359.
[17] F. Weng, C. Chen, H. Yu, Research status of laser cladding on titanium and its alloys: A review, Mater. Des. 58 (2014) 412–425.
[18] J. Dai, F. Zhang, A. Wang, H. Yu, C. Chen, Microstructure and properties of Ti-Al coating and Ti-Al-Si system coatings on Ti-6Al-4V fabricated by laser surface alloying, Surf. Coat. Technol. 309 (2017) 805–813.
[19] H.P. Xiong, W. Mao, Y.H. Xie, W.L. Ma, Y.F. Chen, X.H. Li, J.P. Li, Y.Y. Cheng, Liquid-phase siliconizing by Al–Si alloys at the surface of a TiAl-based alloy and improvement in oxidation resistance, Acta Mater 52 (9) (2004) 2605–2620.
[20] C. Chen, X. Feng, Y. Shen, Oxidation behavior of a high Si content Al–Si composite coating fabricated on Ti–6Al–4V substrate by mechanical alloying method, J. Alloys Compd 701 (2017) 27–36.
[21] C. Badini, S.M. Deambrosis, O. Ostrovskaya, V. Zin, E. Padovano, E. Miorin, M. Castellino, S. Biamino, Cyclic oxidation in burner rig of TiAlN coating deposited on Ti-48Al-2Cr-2Nb by reactive HiPIMS, Ceram. Int. 43 (7) (2017) 5417–5426.
[22] Y. Li, C. Chen, T. Han, J. Ranabhat, X. Feng, Y. Shen, Microstructures and oxidation behavior of NiCrAlCoY-Al composite coatings on Ti-6Al-4V alloy substrate via high-energy mechanical alloying method, J. Alloys Compd 697 (2017) 268–281.
[23] A. Ebach-Stahl, C. Eilers, N. Laska, R. Braun, Cyclic oxidation behaviour of the titanium alloys Ti-6242 and Ti-17 with Ti–Al–Cr–Y coatings at 600 and 700°C in air, Surf. Coat. Technol. 223 (2013) 24–31.
[24] S. Sarkar, S. Datta, S. Das, D. Basu, Oxidation protection of gamma-titanium aluminide using glass–ceramic coatings, Surf. Coat. Technol. 203 (13) (2009) 1797–1805.
[25] I. Gurrappa, A.K. Gogia, High performance coatings for titanium alloys to protect against oxidation, Surf. Coat. Technol. 139 (2) (2001) 216–221.
[26] J. Musil, Hard nanocomposite coatings: Thermal stability, oxidation resistance and toughness, Surf. Coat. Technol. 207 (2012) 50–65.
[27] J. Musil, G. Remnev, V. Legostaev, V. Uglov, A. Lebedynskiy, A. Lauk, J. Procházka, S. Haviar, E. Smolyanskiy, Flexible hard Al-Si-N films for high temperature operation, Surf. Coat. Technol. 307 (2016) 1112–1118.
[28] K.A. Kuptsov, P.V. Kiryukhantsev-Korneev, A.N. Sheveyko, D.V. Shtansky, Structural transformations in TiAlSiCN coatings in the temperature range 900–1600°C, Acta Mater 83 (2015) 408–418.
[29] M. Braun, Magnetron sputtering technique, Handbook of Manufacturing Engineering and Technology, 2015, pp. 2929–2957.
[30] B. Ramamoorthy, An investigation into the adhesion strength of diamond like carbon multilayer coating (DLC/TiN/Ti/Cu/Ni), Intell Inf Manage 01 (03) (2009) 179–194.
[31] C.-C. Chang, J.-G. Duh, Duplex coating technique to improve the adhesion and tribological properties of CrAlSiN nanocomposite coating, Surf. Coat. Technol. 326 (2017) 375–381.
[32] P.W. Shum, Z. Zhou, K.Y. Li, Enhancement of adhesion strength and tribological performance of pure carbon coatings on Ti-6Al-4V biomaterials with ion implantation pre-treatments, 2007.
[33] J. Gerth, U. Wiklund, The influence of metallic interlayers on the adhesion of PVD TiN coatings on high-speed steel, Wear 264 (9) (2008) 885–892.
[34] K.D. Bakoglidis, S. Schmidt, G. Greczynski, L. Hultman, Improved adhesion of carbon nitride coatings on steel substrates using metal HiPIMS pretreatments, Surf. Coat. Technol. 302 (2016) 454–462.
[35] Z. Peng, M. Rohwerder, P.P. Choi, B. Gault, T. Meiners, M. Friedrichs, H. Kreilkamp, F. Klocke, D. Raabe, Atomic diffusion induced degradation in bimetallic layer coated cemented tungsten carbide, Corros. Sci. 120 (2017) 1–13.
[36] X. Chen, H. Gao, Y. Bai, H. Yang, Thermal failure mechanism of multilayer brittle TiN/CrAlN films, Ceram. Int. 44 (7) (2018) 8138–8144.
[37] E. Zoestbergen, J. van de Langkruis, T.F.J. Maalman, E. Batyrev, Influence of diffusion on the coating adhesion of zinc-magnesium thin films onto steel, Surf. Coat. Technol. 309 (2017) 904–910.
[38] J.M. Byun, S.R. Bang, H.W. Kim, T.Y. Kim, S.J. Hong, Y.D. Kim, Effect of heat treatment on corrosion resistance and adhesion property in Zn-Mg-Zn multi-layer coated steel prepared by PVD process, Surf. Coat. Technol. 309 (2017) 1010–1014.
[39] T. Guo, J. He, X. Pang, A.A. Volinsky, Y. Su, L. Qiao, High temperature brittle film adhesion measured from annealing-induced circular blisters, Acta Mater 138 (2017) 1–9.
[40] F. Ahmed, K. Bayerlein, S.M. Rosiwal, M. Göken, K. Durst, Stress evolution and cracking of crystalline diamond thin films on ductile titanium substrate: Analysis by micro-Raman spectroscopy and analytical modelling, Acta Mater 59 (14) (2011) 5422–5433.
[41] F. Cverna, ASM Ready Reference Thermal Properties of Metals, ASM International, Materials Park, Ohio, 2002.
[42] S. M.Johnson, D. J.Rowcliffe, Mechanical properties of joined silicon nitride, J. Am. Ceram. Soc. 68 (1985) 468–472.
[43] W.W. Xu, S.L. Shang, B.C. Zhou, Y. Wang, L.J. Chen, C.P. Wang, X.J. Liu, Z.K. Liu, A first-principles study of the diffusion coefficients of alloying elements in dilute alpha-Ti alloys, Phys. Chem. Chem. Phys. 18 (25) (2016) 16870–16881.
[44] J.W. Lu, Y.Q. Zhao, P. Ge, H.Z. Niu, Microstructure and beta grain growth behavior of Ti–Mo alloys solution treated, Mater. Charact. 84 (2013) 105–111.
[45] Z. Gao, Y. Chen, J. Kulczyk-Malecka, P. Kelly, Y. Zeng, X. Zhang, C. Li, H. Liu, N. Rohbeck, P. Xiao, Comparison of the oxidation behavior of a zirconium nitride coating in water vapor and air at high temperature, Corros. Sci. 138 (2018) 242–251.
[46] R. Wei, E. Langa, C. Rincon, J.H. Arps, Deposition of thick nitrides and carbonitrides for sand erosion protection, Surf. Coat. Technol. 201 (7) (2006) 4453–4459.
[47] J.W.H.D.F. Bahr, N.R. Moody, W.W. Gerberich, Adhesion and acoustic emission analysis of failures in nitride films with a metal, Acta Mater 45 (1997) 5163–5175.
[48] M. Golizadeh, K.A. Kuptsov, N.V. Shvyndina, D.V. Shtansky, Multilayer SiBCN/TiAlSiCN and AlO_x/TiAlSiCN coatings with high thermal stability and oxidation resistance, Surf. Coat. Technol. 319 (2017) 277–285.
[49] A.P. Lange, X.L. Tan, C.S. Fadley, S. Mahajan, Structure and chemistry of aluminum predose layers in AlN epitaxy on (111) silicon, Acta Mater 115 (2016) 94–103.
[50] W.-S.C. Yoon-Suk Oh, Chang-Sam Kim, Dae Soon Lim, Deock-Soo Cheong, XPS investigation of Si_3N_4/SiC nanocomposites prepared using a commercial polymer, J. Am. Ceram. Soc. 82 (1999) 1076–1078.
[51] X.T. Li, L.J. Huang, S.L. Wei, Q. An, X.P. Cui, L. Geng, Cycle oxidation behavior and anti-oxidation mechanism of hot-dipped aluminum coating on TiBw/Ti6Al4V composites with network microstructure, Sci. Rep. 8 (1) (2018) 5790.
[52] M. Paulasto, J.K. Kivilahti, F.J.J. van Loo, Interfacial reactions in Ti/Si_3N_4 and TiN/Si diffusion couples, J. Appl. Phys. 77 (9) (1995) 4412–4416.
[53] Y. Paransky, I. Gotman, E.Y. Gutmanas, Reactive phase formation at AlN–Ti and AlN–TiAl interfaces, Mate. Sci. Eng. A 277 (1) (2000) 83–94.
[54] B. Holmberg, Structural studies on the titanium-nitrogen system, Acta Chem. Scand 16 (1962) 1255–1261.
[55] O. Tunckan, H. Yurdakul, S. Turan, Identification and quantification of reaction phases at Si_3N_4–Ti interfaces by using analytical transmission electron microscopy techniques, Ceram. Int. 39 (2) (2013) 1087–1095.
[56] I. G., E.Y. G., Interaction of Si_3N_4 with titanium powder, J. Mater. Sci. Lett. 9 (1990) 813–815.

[57] M. Maeda, M. Naka, Interfical reaction between titanium and silicon nitride during solid state diffusion bonding Trans, JWRI 30 (2001) 59–65.
[58] L. Esposito, A. Bellosi, G. Celotti, Silicon nitride-nickel joints through diffusion bonding, Acta Mater 45 (12) (1997) 5087–5097.
[59] X. Wang, Y. Yang, X. Luo, W. Zhang, N. Jin, Z. Xiao, G. Feng, Effect of C/Mo duplex coating on the interface and mechanical properties of SiC_f/Ti6Al4V composites, Mate. Sci. Eng. A 566 (2013) 47–53.
[60] Y. Mishin, C. Herzig, Diffusion in the Ti–Al system, Acta Mater 48 (2000) 589–623.
[61] H. Weiss, Adhesion of advanced overlay coatings: mechanisms and quantitative assessment, Surf. Coat. Technol. 71 (2) (1995) 201–207.
[62] A.B. M., C. Arshad, A. Javaid, A. Rafiq, M. Usman, I.H. K., Theory ofadhesion and its practical implications a critical review, J Faculty Eng Technol (2007-2008) 21–45.
[63] J.R. Nicholls, Designing oxidation-resistant coatings, JOM 52 (2000) 28–35.
[64] S.H. Sheng, R.F. Zhang, S. Vepřek, Decomposition mechanism of $Al_{1-x}Si_xN_y$ solid solution and possible mechanism of the formation of covalent nanocrystalline AlN/Si_3N_4 nanocomposites, Acta Mater 61 (11) (2013) 4226–4236.
[65] M.C. Bechelany, V. Proust, C. Gervais, R. Ghisleni, S. Bernard, P. Miele, In situ controlled growth of titanium nitride in amorphous silicon nitride: a general route toward bulk nitride nanocomposites with very high hardness, Adv. Mater. 26 (38) (2014) 6548–6553.
[66] J.P. Roland Hauert, Lukas Knoblauch, Matthieu Diserens, New Coatings by Nanostructuring, Adv. Mater. (Weinheim, Ger.) 11 (1999) 175–177.
[67] A. Pélisson-Schecker, H.J. Hug, J. Patscheider, Morphology, microstructure evolution and optical properties of Al–Si–N nanocomposite coatings, Surf. Coat. Technol. 257 (2014) 114–120.
[68] X. Luo, Y. Yang, Y. Yu, X. Wang, B. Huang, Y. Chen, Effect of Mo coating on the interface and mechanical properties of SiC fiber reinforced Ti6Al4V composites, Mate. Sci. Eng. A 550 (2012) 286–292.
[69] F. Qin, T. Fan, D. Zhang, Thermodynamic effects of alloying elements on solid-state interfacial reactions in a multicomponent system: theoretical treatment and application in SiC_f/Ti composites, Metall. Mater. Trans. A 40 (2) (2009) 462–471.